Journal of Human Evolution 215-216 (2026) 103842

Contents lists available at ScienceDirect

Journal of Human Evolution

journal homepage: www.elsevier.com/locate/jhevol

Chronological assessments of Quina Neanderthals at De Nadale cave (Italy) using combined uranium-series/electron spin resonance dating of fossil teeth

Wenjing Yu [a, *], Lee J. Arnold [b], Martina Demuro [b], Davide Delpiano [c], Alessandra Livraghi [c, d], Renaud Joannes-Boyau [a], Marco Peresani [c, e]

[a] Geoarchaeology and Archaeometry Research Group, Southern Cross University, Lismore, 2480, NSW, Australia
[b] School of Physics, Chemistry and Earth Sciences, Environment Institute and Institute for Photonics and Advanced Sensing (IPAS), Adelaide University, Adelaide, South Australia, 5005, Australia
[c] Prehistoric and Anthropological Science Unit, Department of Humanities, University of Ferrara, 44121, Ferrara, Italy
[d] UMR 5608 TRACES, Université Toulouse Jean Jaurès, 31058, Toulouse, France
[e] Institute of Environmental Geology and Geoengineering, National Research Council, 20133 Milano, Italy

ARTICLE INFO

Article history:
Received 28 July 2025
Accepted 7 April 2026
Available online xxx

Keywords:
Direct dating
Neanderthal
Middle Paleolithic
MIS 4
Late Pleistocene
Quina Mousterian

ABSTRACT

De Nadale Cave is a Neanderthal site located in the Berici Hills of Northeast Italy that provides important insights into regional Middle Paleolithic occupational dynamics. This paper presents the results of the first combined uranium-series and electron spin resonance (U-S/ESR) dating study of herbivore teeth recovered from the site. Three bovid and cervid teeth yield U-S/ESR ages of 79 ± 9 ka, 72 ± 11 ka, and 55 ± 11 ka, with a calculated weighted mean age of 70.1 ± 5.9 ka. These age estimates align with, and further clarify, earlier biochronological findings at De Nadale Cave, as well as previous analyses of charcoal fragments and U/Th dating undertaken on a large herbivore tooth from the site. The new U-S/ESR ages are statistically indistinguishable from the previously published U/Th minimum age of 70.2 +1.0/−0.9 ka when considering their 2σ uncertainty ranges. The consistency of these results supports the reliability of the U-S/ESR chronological framework at De Nadale and indicates that Neanderthal occupation of the site potentially occurred close to the transition between late Marine Isotope Stage (MIS) 5 and early MIS 4, providing important insights into Neanderthal occupation patterns during the harsh stadial and transitional climate phases of the Late Pleistocene. More broadly, the improved chronological framework for De Nadale indicates that Middle Paleolithic Quina technology is likely associated with this MIS transition, in accordance with emerging chronological findings from similar archaeological sites across Western Europe.

© 2026 The Authors. Published by Elsevier Ltd. This is an open access article under the CC BY license (http://creativecommons.org/licenses/by/4.0/).

1. Introduction

Establishing reliable chronologies for Neanderthals and their behavioral traits is a fundamental step in reconstructing the geographic extent and temporal variability of Middle Paleolithic lithic industries across Europe. A key example of this Middle Paleolithic diversity is the Quina (Quina Mousterian) technocomplex, which represents an optimal case study for examining and disentangling the complexity of related technical behaviors. Its initial identification, which served to define a facies of the 'Charentian,' a Mousterian industry particularly common in the Charente region of southwestern France, was based on the high frequency of retouched tools and the presence of scrapers with scaled and deep retouch (Bordes and Bourgon, 1951; Bordes, 1984), which was later refined following studies of core reduction sequences (Bourguignon, 1996, 1997). The chronological and cultural significance of the Quina complex has long been debated, especially in southwestern Europe. Here, its association with cold and arid climatic conditions was originally highlighted in the second half of the 20th century based on faunal assemblages mainly represented by reindeer and secondarily by bisons and horses and on its consistent occurrence within pedosedimentary sequences attributed to the cold stages of the Würm glacial period (Laville,

* Corresponding author.
E-mail address: wenjing.yu@scu.edu.au (W. Yu).

https://doi.org/10.1016/j.jhevol.2026.103842
0047-2484/© 2026 The Authors. Published by Elsevier Ltd. This is an open access article under the CC BY license (http://creativecommons.org/licenses/by/4.0/).

1973; Rolland, 1981). As such, ecological interpretations of the Quina complex have consistently emphasized a close relationship between technological choices and environments, reinforcing the idea of an adaptive cultural response to stadial conditions.

These behaviors are intimately related to late Neanderthals who inhabited Western Europe during Marine Isotope Stage 4 (MIS 4, ~70–60 ka) (Lisiecki and Raymo, 2005), as attested by a few European sites in France, Spain, and Italy that have yielded human remains. The best known is La Quina (Charente, France; Frouin et al., 2017a,b), with 53 hominin remains from a single adult skeleton, a juvenile cranium, and 27 bone and teeth fragments. Among additional findings from levels L to N, large fragments of occipital bones are notable because they provided important information about Neandertal affinities (Verna et al., 2012). Les Pradelles (Charente, France) (Maureille et al., 2010) is also of particular interest, thanks to its numerous hominin fragments of skulls and jaws, isolated teeth, and several postcranial bones, many of them bearing evidence of perimortem manipulations. Among the remains dated to ~60 ka (Frouin et al., 2017a,b), the teeth specimens provide valuable information about the morphology, biology, ethology, and health conditions of the Quina Neanderthal groups in southwestern France (Garralda et al., 2023). In Italy, Neanderthal fossils from Quina Mousterian sites are rare for this time period and are limited to a lower first deciduous molar (Nadale 1) found at De Nadale cave (Grotta De Nadale) in the subalpine region of Northern Italy (Arnaud et al., 2017). Nadale 1 represents a unique source of information on dimensional and morphological variability of Neanderthal lower first deciduous molars (dM_1s) (Arnaud et al., 2017), of oral microbiome, and of weaning timeframes. In particular, the analysis of dental biofilm metagenome shows similarity with modern humans, including acquisition of starch digestion capability in oral streptococci, suggesting microbial coadaptation with host diets (Fellows Yates et al., 2021). Nava et al. (2020) inferred from isotope and histological analyses that Neanderthals started to wean children at 5–6 months. However, aside from these contexts, Quina Neanderthal remains from other sites (in France: Pech de l'Azé IV, Roc-de-Marsal, Hauteroche) still lack a solid chronological position, and De Nadale Cave is no exception.

To improve the chronological framework of the Nadale 1 tooth and its ecocultural context, we present here the results of a combined uranium-series and electron spin resonance (U-S/ESR) dating study of animal tooth remains associated with the Quina lithic assemblage at De Nadale Cave. Our chronological findings are significant for understanding broader regional occupation dynamics as De Nadale Cave is not the first documented example of Quina Mousterian in this geographic region (Fig. 1). Indeed, Quina assemblages from units BR4-BR5 and BR6 at Fumane Cave (FC) in the Lessini Mountains, alongside similar evidence at Ghiacciaia Cave in the Berici Mounts, contribute to the broader chronocultural picture of northeastern Italy, though the exact timing of these Quina occupations in and around MIS 4 remains unclear (Bertola et al., 1999; Bertola and Peresani, 2000; Peresani, 2022, 2023; Falguères et al., 2025).

Establishing reliable chronological frameworks for the Quina technocomplex remains challenging due to the scarcity of well-preserved stratified contexts and the limitations of conventional dating methods. In this paper, we provide the first U-S/ESR ages on tooth enamel for De Nadale Cave, which had previously only been chronologically constrained using U/Th dating of a large herbivore tooth that yielded a minimum age of 70.2 +1.0/−0.9 ka (Jéquier et al., 2015).

2. Site context

The study area is situated in Northeastern Italy, encompassing parts of the Veneto and Friuli Venezia Giulia regions, which are characterized by diverse geomorphological features, including Alpine massifs, river valleys, karstic plateaus, and sub-Alpine mountains. These varied landscapes create diverse ecological settings that have attracted human settlement throughout prehistory, with many key sites offering insights into early human occupation during the Middle and Late Pleistocene period (Peresani, 2001, 2023; Margaritora et al., 2020).

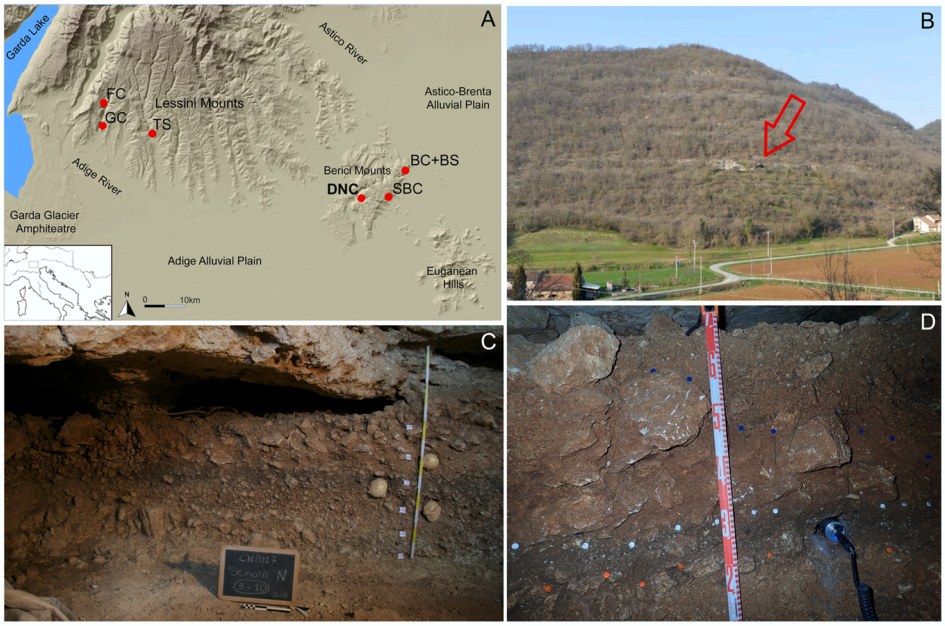

Figure 1. (A) Digital terrain model (DTM) of north-eastern Italy showing the location of De Nadale Cave (DNC) and other major Paleolithic sites in the region: San Bernardino Cave (SBC), Broion Cave (BC), Broion Shelter (BS), Fumane Cave (FC), Ghiacciaia Cave (GC), and Tagliente Shelter (TS); (B) the southern slope of the Berici Plateau in the Liona Valley, with the location of the site indicated; (C) stratigraphic section of the deposit, highlighting the dark SU 7 exposed at the start of the 2017 excavation campaign in sqs. M13 to O13; (D) sampling location for associated dose-rate measurements. (For interpretation of the references to color in this figure, the reader is referred to the web version of this article.)

In particular, the Berici Mounts (Colli Berici) area is of interest for investigating the interaction between early human groups and environmental features of the region (Fig. 1). The Berici span a territory of about 200 km^2, reaching the highest point at 444 m above modern sea level. Characterized by a combination of fluvial and karst formations, the Berici morpho-unit is the result of a prolonged evolution history (Mietto and Sauro, 2000; Sauro, 2005, 2016), which was strongly influenced by the lithological characteristics and structural configuration of the underlying Upper Cretaceous to the Lower Miocene bedrock. The sedimentary formations include marly limestones (Scaglia Rossa, Scaglia Cinerea, Marne Euganee, and Formazione di Priabona), which are highly erodible and extensively exposed in the western sector, carbonate biodetritical sandstones (Pietra di Nanto and Arenarie di Sant'Urbano), calcarenites rich in nummulites (Calcari Nummulitici), bioconstructed limestones (Castelgomberto Formation), and basaltic flows, interspersed with volcanoclastic deposits (tufa and explosive volcanic breccia), residual clayey deposits, and coastal carbonate sandstones (Orizzonte a *Cerithium diaboli*) (Mietto, 1988; Bassi, 2000; Mietto and Sauro, 2000; Tusberti et al., 2024).

Notable archaeological sites in the area include caves such as De Nadale Cave, Broion Cave, Broion Rock Shelter, San Bernardino Cave, Fumane Cave, Ghiacciaia Cave, and Tagliente Shelter, which have all yielded evidence of past human activities (Peresani, 2001, 2015; Terlato et al., 2021) (Fig. 1). Their sedimentary sequences record the principal external and internal processes that shaped the evolution of the karst slopes and valleys: rockfall, éboulis accumulation, soil and sediment colluviation, aeolian sedimentation, accumulation of residual sands, coarser particles, and geogenic material (Marcazzan, Arnold et al., in prep.). The De Nadale Cave (45° 25′ 16″ N; 11° 29′ 22″ E) is a particularly important site due to its Mousterian deposit and well-preserved stratigraphy. Discovered in 2006, subsequent excavations have uncovered a key stratigraphic sequence, with unit 7 containing the primary layer (Jéquier et al., 2015).

The cave lies within a landscape dissected by the Calto Valley bottom, characterized by small valleys and seasonal streams that supported historical mills. Eight archaeological excavations were conducted from 2014 to 2021. These revealed a short stratigraphic sequence that includes a single Middle Paleolithic anthropic layer (unit 7), bounded above and below by archaeologically sterile deposits (units 3, 6, and 8). Unit 3 is a thick layer alternating between stony loamy textured layers and loose breccia composed of medium- to-large-sized carbonate elements, tabular, tilted according to the boundaries of the unit. Unit 3 covers unit 6, rubble made of large subangular and tabular stones with a subhorizontal arrangement. Unit 7 is dark-brown- to gray-colored silt loam with crumbly aggregation and medium- to small-sized subrounded carbonate stones. Unit 8 is a loose stone-supported breccia with silt-clay matrix and stones coated with blackish iron and manganese stains on their upper faces. Unit 9 is a thin residual clayey layer produced by active dissolution of the bedrock. Fourier-transform infrared spectra of two sediment samples from squares N11 and Q12 showed peaks of carbonate—hydroxyapatite that indicate alkaline/subalkaline contexts, despite the presence of montmorillonite, kaolinite, and organic matter that tend to form in typically acidic conditions. In general, excellent preservation of the osteological material has been observed, with bones from the eastern zone appearing light colored and fragile, while fragments from the western zone are brownish in color and have a more solid texture (Livraghi et al., 2021). This layer yielded the Neanderthal dM_1 (Arnaud et al., 2017) and contained a variety of artifacts, including lithic tools and animal remains attributable to Neanderthal occupations (Jéquier et al., 2015).

The lithic assemblage is categorized as Quina Mousterian based on the recurrent reduction of cores for producing thick flakes, usually characterized by three or more orders of stepped-scaled retouch (Peresani et al., 2023). The Quina assemblage of De Nadale has been referred to as 'atypical,' given some differences in core-reduction patterns, partly because of the high reduction rate and fragmentation of the assemblage (Delpiano et al., 2022). On the other hand, blank manufacturing and transformation cycles, which include their use and instances of ramified behavior, typically adhere to the Quina concept. The site's environmental context, including the presence of springs and moist zones, offers further insights into human settlement patterns (Vidal-Matutano et al., 2022).

Zooarchaeological studies conducted at De Nadale Cave have identified an intensive set of hunting and butchering activities, mainly focused on large- and medium-to-large-sized species. Evidence suggests that red deer (*Cervus elaphus*), giant deer (*Megaloceros giganteus*), and large-sized bovids (*Bison priscus* and *Bos primigenius*) were the most exploited species, with a notable presence of several anthropic modifications aimed at meat and tendon recovery, marrow extraction, and other activities related to carcass exploitation (Terlato et al., 2019; Livraghi et al., 2021). The hunting season was most likely correlated with winter, as demonstrated by dental wear pattern and cementum analysis (Livraghi et al., 2022). Additionally, more than 300 retouches made using cervid and bovid bones were found in the area (Martellotta et al., 2021). Based on the micromammal assemblages found in the cave, represented by *Microtus arvalis*, *Microtus agrestis*, and *Chionomys nivalis*, the biochronology indicates a cold, dry climate with some humid areas in the valley bottoms, which is consistent with the attribution to MIS 4 (71 ka to 57 ka) (López-García et al., 2018). However, MIS 4 is not well documented in European continental records, and U/Th dating of the unit 7 tooth (Jéquier et al., 2015) only provides a minimum age estimate due to open-system postmortem U-uptake dynamics. Therefore, additional direct dating of fossil material from De Nadale unit 7 is crucial in this context.

3. Material and methods

Electron spin resonance dating is a paleodosimetric method that evaluates the effects of natural radioactivity accumulated by a sample, allowing the dating of a wide range of fossil teeth from different geological settings (Shao, 2011; Duval, 2015; Dirks et al., 2017; Pereira et al., 2017; Richter et al., 2017; Han et al., 2019; Ben Arous et al., 2020; Rizal et al., 2020; Withnell et al., 2020;Hakim et al., 2025). When ESR measurements are combined with uranium series data, namely U-S/ESR dating, the resulting age estimates are improved by mathematically accounting for the complexities of postmortem uranium uptake. (For fundamental models, see Bischoff and Rosenbauer, 1981; Ikeya, 1982; Blackwell et al., 1992). Combined uranium-series and electron spin resonance dating has traditionally been used to date Middle to Late Pleistocene remains older than the upper limit of radiocarbon (>~50 ka), though some research has also shown that it has the potential for dating up to 2.6 or even 3 million years (e.g., Herries et al., 2018; Yu et al., 2024). This combined method has been widely applied at archaeological sites across Europe, consistently yielding promising results (e.g. Michel et al., 2009; Liberda et al., 2010; Richter et al., 2017; Bahain et al., 2020, 2021; Falguères et al., 2025). Although the precision of U-S/ESR dating is not as high as radiometric dating methods such as radiocarbon, uranium-series (U-Pb and U-Th), or argon-argon (Ar-Ar) (Duval et al., 2020), recent research suggests that U-S/ESR dating is at least comparable in accuracy to radiocarbon dating (Richard et al., 2020), Ar-Ar dating (Bahain et al., 2021), and optically stimulated luminescence (OSL) dating (Ben Arous et al., 2020).

3.1. Sample preparation and irradiation

The U-S/ESR dating analysis was conducted on three fossil teeth recovered from unit 7 of De Nadale Cave: one bovid specimen (CN-857, Q 12) and two cervid specimens (CN-1322 and CN-55, N11) (See Supplementary Online Material [SOM]). Sample CN-857 was collected during the 2017 excavation campaign, while CN-55 and CN-1322 were obtained during the 2014–2015 field seasons (Figs. 2 and 3). A series of tooth enamel powder samples were prepared and analyzed following the requirements of the U-S/ESR dating protocols on teeth (Joannes-Boyau et al., 2010; Duval, 2015; Richard et al., 2017). The teeth were collected by A. Livraghi during the archaeological excavation (Table 1).

Each tooth was first examined to identify and avoid areas showing obvious diagenetic alteration, and enamel thickness was measured prior to sampling. The specimen was then cut into two halves, and the enamel was carefully separated from the surrounding dentine and any adhering external deposits using a diamond saw. A minimum of 70 μm of enamel was removed from all enamel surfaces to eliminate potential external contamination (Table 1).

One half of the cleaned enamel was subsequently crushed into powder, split into 10 aliquots (approximately 50–70 mg each), and sent for gamma irradiation prior to ESR dose determination. The remaining half of the sample was reserved for U-series analysis.

Gamma irradiations were performed on powdered samples using a calibrated ^{60}Co gamma source with a dose rate of 23.8 Gy/min at the Australian Nuclear Science and Technology Organization, Australia. Powder samples were gamma irradiated to the following doses for each sample: 10 Gy, 20 Gy, 50 Gy, 100 Gy, 250 Gy, 600 Gy, 1200 Gy, 2400 Gy, and 3500 Gy. However, due to limited sample availability, only a subset of irradiation steps could be applied to some samples.

3.2. Equivalent dose determination

Electron spin resonance intensities of the prepared aliquots were measured at room temperature using a Freiberg MS5000 ESR spectrometer (Friberg, Germany) at Southern Cross University. The following parameters were used for all measurements: 2-mW microwave power, 100-kHz modulation frequency with 1024 points resolution, 0.1-mT modulation amplitude, 45-second conversion time, 12-mT sweep width, and 21-second sweep time. The ESR intensities of enamel powder were extracted using peak-to-peak (TI-B2) integration, following the method by Duval and Grün (2016). Equivalent dose (D_E) values and dose–response curves (DRCs) were obtained by fitting a single saturated exponential (SSE) function in the fitting program McDose 2 (Joannes-Boyau et al., 2018), following the recommendations of Duval et al. (2013).

3.3. Uranium-series data

High-resolution U-series analyses of the enamel and dentine were performed on the remaining half of each tooth. The concentrations of ^{238}U, ^{234}U, and ^{230}Th were determined by laser ablation multi collector inductively coupled plasma mass spectrometry (LA-ICP-MS) using the ESI NW193 ArF Excimer (Electro Scientific Industries, Portland, USA). For each sample, several raster scans (laser ablation tracks) were performed across both the enamel and dentine. The LA-ICP-MS parameters included a spot size of 100 μm, a frequency of 20 Hz, a scan speed of 5 μm/s, and an energy density of approximately 7.3 J/cm^2. Each ablation with measurements taken along a series of parallel tracks aligned with the growth axis of the dental tissues. Signal drift was monitored using certified reference materials NIST610, NIST612 MK 10, and MK 16. (For details, see Slimak et al., 2024; Joannes-Boyau et al., 2025). For each tissue type (enamel and dentine), an average U and Th concentration obtained by LA-ICP-MS was calculated by merging several rasters and used for the optimal U-uptake model in the age calculations (Table 1).

3.4. Age calculation

This research uses the uranium uptake (US)-ESR model, which allows the uranium uptake history to be mathematically modeled using a *p* value derived from combined ESR and U-series data to

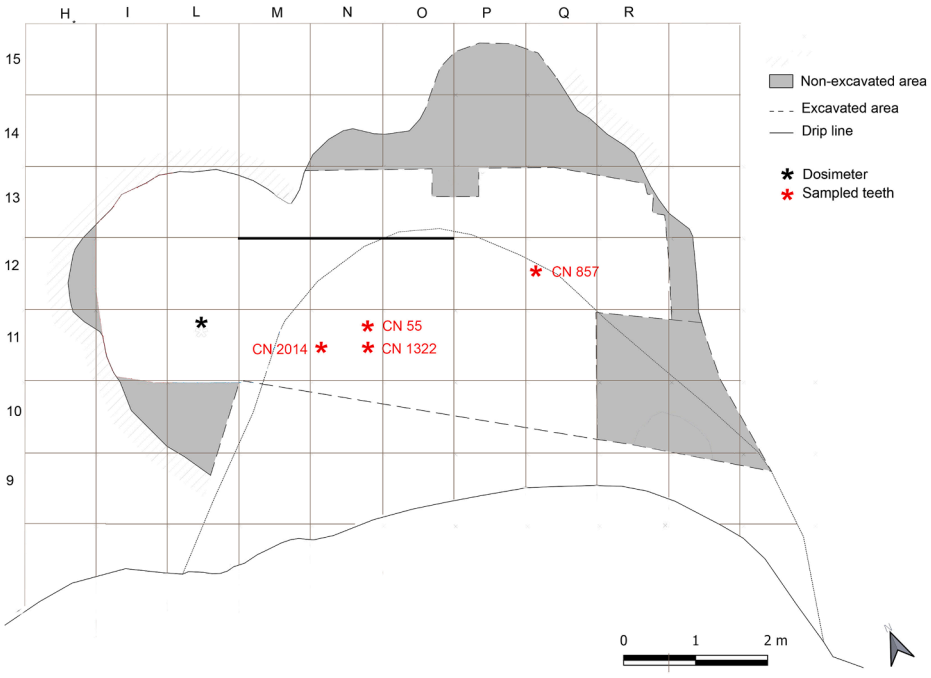

Figure 2. Planimetry of De Nadale Cave at present-day showing the sample locations of CN-55 and CN-1322 (square N11h) and CN-857 (square Q12b) within unit 7. Letters and numbers refer to the excavation grid squares. The in situ gamma dosimeter was placed in square L11. The position of the photographed and drawn stratigraphic section of the deposit is indicated in squares M13–N13–O13. (For interpretation of the references to color in this figure, the reader is referred to the web version of this article.)

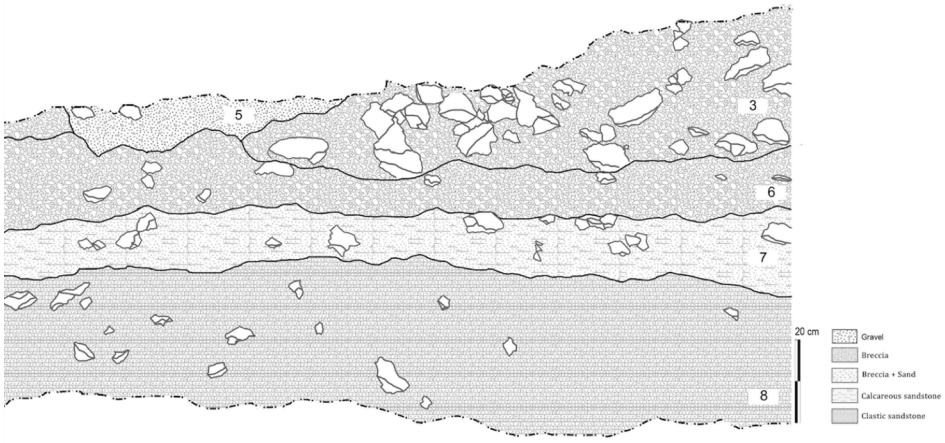

Figure 3. Detailed drawing of the stratigraphic section.

obtain a consistent age estimate (Grün et al., 1988). The following parameters were used for U-S/ESR age calculation (Shao et al., 2014) (1σ uncertainties): alpha-efficiency of 0.13 ± 0.02 (Grün and Katzenberger-Apel, 1994), dose–rate conversion factors from Adamiec and Aitken (1998), a water content of 3 wt % ± 3 wt% in the enamel, 5 wt% ± 5 wt% error in the dentine, and none in cementum. Beta attenuation in the enamel layers follows Brennan et al. (1997). Of note, Rn and Ra loss was not measured within the dental tissue, but equilibrium was assumed (Joannes-Boyau, 2014; Dirks et al., 2017; Yu et al., 2024).

Representative external gamma-dose-rate measurements were obtained for the tooth samples at De Nadale Cave by performing in situ gamma spectrometry measurements in unit 7 (excavation square L11, section South; Figs. 1D and 2), approximately 1.5 m from the western wall and located 2 m from fossil tooth samples CN-55 and CN-1322, and 4.5 m from sample CN-857, using a Canberra Inspector 1000 and 2-inch Na:I probe. Elemental concentrations of K, U, and Th were determined from the field gamma-ray spectra using the 'energy windows' method described in Arnold et al. (2012) and Duval and Arnold (2013). These elemental concentrations were then used to calculate the gamma dose rates, enabling us to capture any spatial heterogeneity in the surrounding (~30-cm diameter) gamma radiation field.

Sediment beta dose rates were determined from U, Th, and K activities obtained using high-resolution gamma spectrometry (HRGS) measurements performed on dried and homogenized bulk sediment collected directly from the unit 7 gamma spectrometry hole position. The bulk sediment sample was dried at 90 °C for 2 days and ground to <1 μm using a planetary ball mill (400 rpm for 15 minutes) to ensure homogenization prior to analysis. Approximately 7 g of the powdered sediment was sealed in a plastic container for at least 30 days (equivalent to eight half-lives of ^{222}Rn; $t_{1/2}$= 3.825 days) to allow postradon daughters (^{214}Pb and ^{214}Bi) to reach equilibrium with parent ^{226}Ra activities. Gamma spectrometry measurements were conducted using a p-type, high-purity germanium well detector following the procedures outlined by Leslie (2009).

A present-day sediment water content of 9.8% (wet weight) was obtained from the bulk sediment sample collected from the unit 7 gamma spectrometer hole. This value has been used to approximate the long-term sediment content for the U-S/ESR age calculations, and a 1σ relative uncertainty of 25% has been assigned to the long-term moisture estimates to accommodate any variations in hydrologic conditions during burial.

Cosmic-ray dose rates were calculated using the approach described in Prescott and Hutton (1994), taking into consideration site altitude; geomagnetic latitude; and density, thickness, and geometry of sediment overburden. The effects of bedrock shielding have additionally been incorporated into the cosmic dose-rate calculation using the present-day rock shelter geometry and the integrated $\cos^2 \phi$-zenith angular dependence procedures outlined in Allkofer (1975) and Smith et al. (1997).

4. Results

4.1. Equivalent dose results

The D_E values, enamel and dentine data details, along with final age estimations for De Nadale Cave, are summarized in Table 1. The ESR DRCs for samples CN-857, CN-1322, and CN-55 all exhibit consistent increases in signal intensity with rising irradiation doses, confirming the reliability of the datasets (Figs. 4–6). Due to the limited amount of available enamel, samples CN-55 and CN-1322 were each irradiated at only five dose steps.

Although all three samples generated statistically similar D_E values (54.9 ± 2.6 Gy for CN-857, 46.3 ± 4.7 Gy for CN-1322, and 41.7 ± 6.7 Gy for CN-55), CN-857 stands out due to its lower relative uncertainty and higher resolution curve. As shown in Figures 4–6, single saturation exponential (SSE) functions provided better fits for the DRCs of CN-857. In the case of CN-1322 and CN-55, the D_E was also derived using the SSE function but based on only six points, leading to a relatively higher uncertainty of approximately 10%.

4.2. Dose-rate evaluation

As shown in Table 1, the enamel uranium concentrations exceeded 1 ppm for samples CN-857 and CN-55, while CN-1322 showed a much lower value (~0.215 ppm), resulting in a reduced internal dose-rate contribution (~3.1%) compared to 10–15% for the other samples. The dentine uranium concentrations ranged from ~17.281 to ~33.928 ppm. Uranium uptake modeling indicates differing histories for the tooth samples: CN-857 and CN-1322 display p values greater than zero, suggesting recent uptake, whereas CN-55 exhibited negative p values in both enamel and dentine, consistent with an early uptake model in which uranium was rapidly incorporated shortly after burial (Han et al., 2017) (Table 1). Further discussions of CN-857 are provided in the SOM. Due to the absence of cementum, its dose-rate contribution was set to zero in the US-ESR program used for age calculation.

Table 1
A summary of the ages calculated from De Nadale fossil tooth samples using the US-ESR program.

	De Nadale		
	CN-857	CN-1322	CN-55
	sq. Q12b—unit 7	sq. N11h—unit 7	sq. N11i—unit 7
Enamel			
Dose (Gy)[a]	54.9 ± 2.6	46.3 ± 4.7	41.7 ± 6.7
U (ppm)	1.059 ± 0.040	0.215 ± 0.091	1.079 ± 0.070
$^{234}U/^{238}U$	1.102 ± 0.050	1.065 ± 0.000	1.091 ± 0.008
$^{230}Th/^{234}U$	0.368 ± 0.007	0.302 ± 0.143	0.364 ± 0.010
Thickness (μm)	1000 ± 100	1100 ± 100	1200 ± 100
Removed Thickness (μm, side 1)	70 ± 20	75 ± 20	80 ± 30
Removed Thickness (μm, side 2)	69 ± 21	73 ± 20	75 ± 25
Water (%)	3 ± 3	3 ± 3	3 ± 3
Dentine			
U (ppm)	18.081 ± 0.283	33.928 ± 2.574	17.281 ± 0.939
$^{234}U/^{238}U$	1.073 ± 0.006	1.069 ± 0.012	1.096 ± 0.006
$^{230}Th/^{234}U$	0.185 ± 0.006	0.259 ± 0.023	0.355 ± 0.008
Water (%)	5 ± 5	5 ± 5	5 ± 5
Sediment			
U (ppm)	2.00 ± 0.23	2.00 ± 0.23	2.00 ± 0.23
Th (ppm)	4.13 ± 0.25	4.13 ± 0.25	4.13 ± 0.25
K (%)	0.50 ± 0.02	0.50 ± 0.02	0.50 ± 0.02
Water (%)	9.80 ± 2.50	9.80 ± 2.50	9.80 ± 2.50
External dose rate (mGy/ka)			
Beta dose	79 ± 10	78 ± 9	71 ± 9
Gamma dose	333 ± 14	333 ± 14	333 ± 14
Cosmic	84 ± 30	84 ± 30	84 ± 30
US-ESR age			
Internal dose rate (mGy/ka)	145 ± 18	19 ± 9	192 ± 30
Beta dose (mGy/ka)	133 ± 11	212 ± 28	189 ± 24
P enamel	−0.49 ± 0.12	−0.27 ± 0.24	−0.9 ± 0.19
P dentine	1.36 ± 0.30	0.07 ± 0.30	−0.86 ± 0.19
Total dose rate (mGy/ka)	694 ± 50	648 ± 55	798 ± 65
Age (ka)	79 ± 9	72 ± 11	55 ± 11

US-ESR: U-S/ESR dating using the uranium uptake (US) model.
The external dose-rate data for samples CN-857, CN-1322, and CN-55 are based on an in situ gamma spectrometry measurement performed in unit 7 (external gamma dose rate) and high-resolution gamma spectrometry measurement of bulk sediment collected from the unit 7 in situ gamma spectrometry hole (external beta dose rates).
[a] Dose (Gy): dose in Gray.

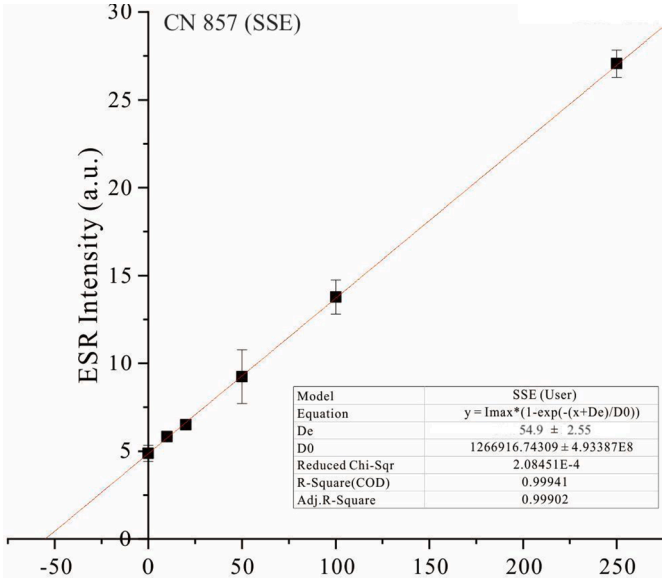

Figure 4. Dose–response curves (DRCs) for samples CN-857 were fitted using a single saturating exponential function (SSE). COD = coefficient of determination; ESR = electron spin resonance. (For interpretation of the references to color in this figure, the reader is referred to the web version of this article.)

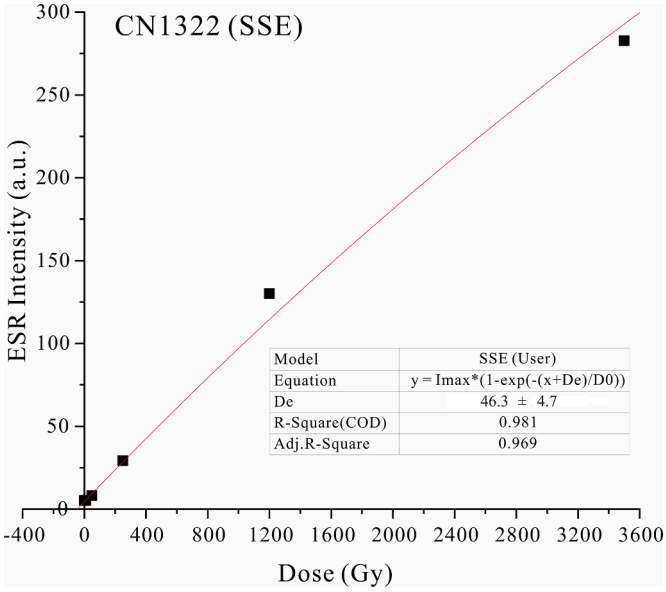

Figure 5. Dose–response curves (DRCs) for samples CN-1322 were fitted using a single saturating exponential function (SSE). COD = coefficient of determination; ESR = electron spin resonance. (For interpretation of the references to color in this figure, the reader is referred to the web version of this article.)

The external dose rate of the fossil tooth samples was derived from the beta and gamma dose rates of the surrounding sediment and cosmic radiation (Table 1). Since all three fossil tooth samples were collected from the same context (unit 7), representative sedimentary dose-rate data have been calculated using the in situ gamma spectrometry and bulk sediment HRGS measurements

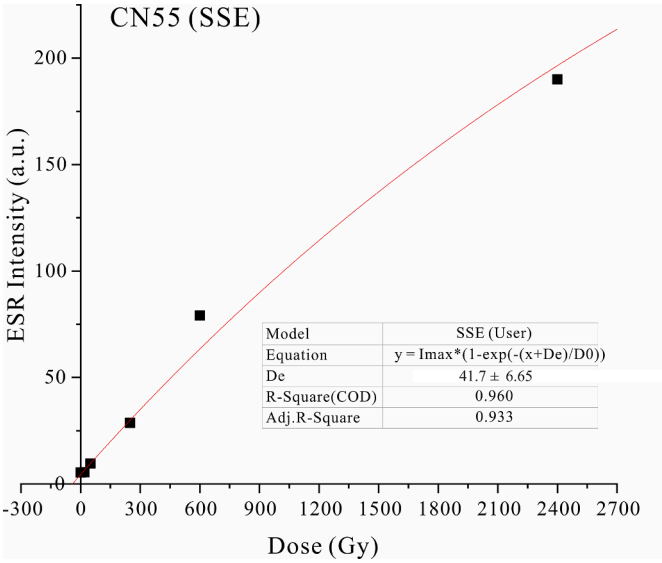

Figure 6. Dose–response curves (DRCs) for samples CN-55 were fitted using a single saturating exponential function (SSE). COD = coefficient of determination; ESR = electron spin resonance. (For interpretation of the references to color in this figure, the reader is referred to the web version of this article.)

taken from a location in square L11 in the southern section, approximately 1.5 m from the western wall of the cavity (Table 1). In using this approach, it is acknowledged that there may be differences between the true gamma dose rates of individual tooth samples and the measured gamma dose rate owing to spatial heterogeneities in limestone clast abundance across different sectors of the site. This consideration may explain some of the variation in the U-S/ESR tooth ages shown in Table 1 as the gamma dose rate carries significant weight in the final age determination, contributing between ~48.2% (CN-55) and ~48.0% (CN-857) to the total dose rate. The HRGS specific activities of ^{238}U, ^{226}Ra, ^{210}Pb, ^{228}Ra, ^{228}Th, and ^{40}K obtained for bulk sediments collected directly from the unit 7 gamma spectrometry hole are summarized in Table 2. These results show that the ^{238}U and ^{232}Th decay chains are broadly in present-day secular equilibrium (i.e., the daughter–parent isotopic ratios are consistent with unity at 2σ). These activities have been used to derive the external beta dose rates shown in Table 1.

4.3. U-S/ESR ages

The results obtained using the US-ESR model are shown in Table 1. Samples CN-857 and CN-1322 produce ages of 79 ± 9 ka and 72 ± 11 ka, respectively, while CN-55 produced a younger age of 55 ± 11 ka. The calculated weighted mean age of the three samples is 70.1 ± 5.9 ka.

4.4. U/Th dating results

Uranium-series (U/Th) dating results for the Nadale Cave sequence are presented in Table 3. The U/Th ages obtained for the dentine are 22.26 ± 1.3 ka (CN-857), 30.58 ± 1.6 ka (CN-1322), and 47.58 ± 1.9 ka (CN-55). In addition, enamel U/Th ages of 44.10 ± 15.6 ka (CN-857) and 49.05 ± 2.8 ka (CN-55) were obtained. The U/Th age for sample CN-2014, previously published by Jéquier et al. (2015), is also included for comparison. This sample derives from the same stratigraphic unit (unit 7) and excavation square (N11) as samples CN-55 and CN-1322 (Fig. 2).

5. Discussion

The U-S/ESR dating results presented in this study provide a more refined chronological framework for the De Nadale site, situating the main human occupation phase at 70.1 ± 5.9 ka. This timeframe most likely corresponds to the transition between late MIS 5 and early MIS 4, which has important implications for understanding Neanderthal behavior and regional occupation dynamics in northern Italy during the Middle Paleolithic.

Overall, the U-series ages obtained in this study, ranging from ~22.3 ka (CN-857 dentine) to ~49.1 ka (CN-55 enamel), are systematically younger than the U-S/ESR age estimates. This relationship is expected as U-series dating typically provides minimum age constraints due to progressive uranium uptake after burial, whereas US-ESR modeling accounts for uranium uptake histories over time. As shown in Table 3, the generally low thorium concentrations (typically <200 ppb) and high ^{230}Th/^{232}Th ratios indicate negligible detrital thorium contamination, supporting the overall reliability of the U-series data. However, samples CN-55 and CN-857 should be treated with caution, as discussed later.

5.1. Errors and uncertainties

The first source of uncertainty may arise from age underestimation in sample CN-55. The DRC of CN-55 exhibits a relatively low adjusted R^2 value (0.933), and the precision of the final D_E estimate is strongly influenced by an outlying fifth dose point (600 Gy). When excluding the fifth and the sixth point, the age increases from 55 ± 11 ka to 75 ± 32 ka (see SOM). In addition, negative *p* values obtained for both the enamel and dentine indicate early uranium uptake or potential uranium leaching, which likely led to an underestimation of the true age when these two points are not excluded from the DRC. This may explain why the CN-55 age is systematically younger than the other two samples, although all three derive from the same site (Table 1). Furthermore, CN-55 exhibits a lower uranium concentration and potentially contradicts the existing U/Th minimum age data for unit 7 as the U-S/ESR age should not be younger than the U/Th minimum age of 70.2 +1/−0.9 ka (Jéquier et al., 2015).

In contrast, CN-1322 appears to be consistent with the U/Th age obtained in the previous study by Jéquier et al. (2015) (Table 3). The dentine uranium concentrations of CN-1322 and CN-2014 are also statistically comparable, as are their U-S/ESR ages. Moreover, the enamel of CN-1322 exhibits a low uranium concentration (~0.215 ppm) and a similar ^{230}Th/^{234}U activity ratio (0.302). However, CN-1322 displays the highest uranium concentration in the dentine among the three samples, which likely reflects tooth-specific microstructural factors or distinct geochemical behavior

Table 2
High-resolution gamma spectrometry (HRGS) results for bulk sediments collected directly from the unit 7 gamma spectrometry hole.

Radionuclide specific activities (Bq/kg)[a,b]						Daughter-to-parent isotopic ratio		
^{238}U	^{226}Ra	^{210}Pb	^{228}Ra	^{228}Th	^{40}K	^{226}Ra:^{238}U	^{210}Pb:^{226}Ra	^{228}Th:^{228}Ra
31.8 ± 2.7	30.4 ± 0.6	27.7 ± 3.9	17.6 ± 0.9	19.9 ± 0.7	178 ± 7	0.96 ± 0.08	0.91 ± 0.13	1.13 ± 0.07

[a] Measurements made on dried and powdered sediment subsamples of ~7 g.
[b] Mean ± total uncertainty (68% confidence interval), calculated as the quadratic sum of the random and systematic uncertainties.

Table 3
Uranium-series analytical results for dentine and enamel.

Sample	Tissue	U (ppm)	±2SE	Th (ppb)	±2SE	$^{234}U/^{238}U$	±2σ	$^{230}Th/^{238}U$	±2σ	$^{230}Th/^{232}Th$	Age (ka)	±1σ
CN-857	Dentine	18.08	0.28	347.8	69.0	1.0726	0.0068	0.1984	0.0064	4500	22.26	1.3
CN-857	Enamel	1.06	0.04	153.0	32.5	1.1125	0.0460	0.3725	0.0705	2555	44.10	15.6
CN-1322	Dentine	33.93	2.58	126.3	39.5	1.0688	0.0127	0.2772	0.0298	5240	30.58	1.6
CN-55	Dentine	17.28	0.94	127.8	40.8	1.0955	0.0125	0.3893	0.0068	4200	47.58	1.9
CN-55	Enamel	1.08	0.07	127.6	36.1	1.0910	0.0080	0.3398	0.0099	3960	49.05	2.8
CN-2014 (Jéquier et al., 2015)	Dentine	31.30	0.10	47.0	2.0	1.0720	0.0030	0.5117	0.0030	1043	70.20	0.9

Concentrations, activity ratios, and ages are reported for individual analyses. Uranium-series ages for the enamel of sample CN-1322 are not reported due to thorium concentrations below the detection limit. Sample CN-2014 was previously analyzed in a U/Th dating study (Jéquier et al., 2015).

relative to the other fossil teeth (Duval and Grün, 2016). Sample CN-857 exhibits comparatively high thorium concentrations in the dentine (>300 ppb), suggesting a more complex geochemical history (Table 3). This may reflect open-system behavior and/or multiple phases of uranium uptake, and therefore the age obtained for this sample should be interpreted with caution.

Another potential source of uncertainty affecting the U-S/ESR ages is the reconstruction of external dose rates. The in situ gamma-dose-rate measurement was performed about 2–4.5 m from the tooth samples in the same stratigraphic level (unit 7). However, this level is relatively heterogenous from a dose-rate perspective owing to the presence of numerous limestone clasts (Fig. 1), and therefore the representativeness of the gamma-dose-rate measurement for other areas of the site cannot necessarily be guaranteed. Similarly, the external beta-dose-rate reconstruction is affected by practical constraints: the fossil teeth were recovered from earlier excavation campaigns, so it was not possible to sample sediment directly adhering to the specimens for external beta-dose-rate evaluation. Instead, bulk sediment was also collected from the unit 7 gamma-dose-rate measurement position. While this provides a general characterization of the depositional environment, it may not fully represent the external beta dose rate at the tooth surface, given the shallow penetration depth of beta radiation (~2 mm) (Duval et al., 2009; Duval and Martin, 2019). An additional potential source of systematic uncertainty affecting the U-S/ESR ages is uranium mobility during burial. This might have resulted in differences between the actual and modeled uranium uptake history (Grün, 2009; Duval and Martin, 2019; Yu et al., 2025). Consequently, both the external gamma and beta dose rates should be regarded as approximations, introducing additional, though unquantified, uncertainty into the final U-S/ESR age estimates.

5.2. Chronological interpretations

Importantly, the occupation of De Nadale falls within the broader temporal range of Quina Mousterian assemblages identified elsewhere in Europe, including at Fumane Cave (Peresani et al., 2023). While De Nadale is unique in its stratigraphic integrity and faunal assemblage, comparison with the Quina levels at Fumane suggests regional synchronicity in technological traditions and possible evidence for the development of technical patterns, given the progressive 'typification' of the Quina Mousterian at Fumane.

Overall, the Quina system is characterized by a branched production cycle that involves flaking cores on alternating and cutting surfaces in various forms, the production of thick and lateralized flakes, and their habitual modification into simple, transverse, or convergent scrapers through scaled and repeated, multilayered retouching. This system is represented in the nearby and well-documented Fumane Cave cultural sequence, particularly in units BR4–BR5 (Peresani et al., 2023), though the closest matchings are found in the reduction schemes and toolkits described by L. Bourguignon and A. Turq in Southwestern France (Turq, 1989, 2000; Bourguignon, 1996, 1997). At De Nadale, the Quina system is characterized by a higher degree of variability related to the minor presence of other flaking methods and a pronounced branching in the production sequences. This pattern closely resembles the behaviors observed in unit BR6 at Fumane Cave, which also potentially shares a comparable chronology with De Nadale (Peresani, 2012; Falguères et al., 2025). However, BR6 remains unpublished in terms of detailed technological analysis and it's still not directly dated. This unit immediately precedes the Quina Mousterian documented in layers BR4–BR5, which, by contrast, is more characteristically aligned with the reference lithic assemblages from Aquitaine, France (Peresani et al., 2023). Taken together, these could imply that Quina technology developed and persisted across varied ecological zones in northern Italy and even southern France, possibly reflecting shared adaptive strategies among dispersed Neanderthal populations (Castel et al., 2024).

The chronological consistency of Quina Mousterian expands from Northern Italy to France and the Iberian Peninsula. The available ages from key European Quina sites place its first occurrences within early MIS 4 in various regions, including Southwestern France at Chez Pinaud-Jonzac layer US022 (thermoluminescence [TL] dating at ~73 ± 3 ka; Richter et al., 2013), northern Iberia at Axlor level D (OSL dating between 75 and 65 ka; Demuro et al., 2023), and southeastern France at Mandrin layer F (OSL dating beginning at 69 ka; Slimak et al., 2022). Numerous Quina sites are dated between MIS 4 and early MIS 3, including La Quina Amont levels G to N (63–55 ka; Frouin et al., 2017a,b) and Pradelles-Marillac UL B (57.6 ± 4.8 ka), both dated with OSL and with statistical chronological models of the sequence based on TL, feldspar infrared stimulated luminescence, U/Th, and ^{14}C data (Maureille et al., 2010; Frouin et al., 2017a,b). This MIS 3 phase also includes the sites of Pech de l'Aze II level 2A-2G and IV level 4A (57.3 ± 2.8 ka), dated with single-grain OSL and previously with TL, ESR, and ^{14}C (Jacobs et al., 2016). In the Balkans, Quina is found at Crvena Stijena levels XXII and XX, dated with OSL and ESR to 65.5–48.3 ka (Mihailović and Whallon, 2017). Quina sites are known from early MIS 3, including Roc de Marsal levels 2–4, dated with TL and OSL (Guérin et al., 2012, 2017), Combe-Capelle Bas levels 1D-1E-2B, dated with TL (Valladas et al., 2003), and finally the later sites at Sous-les-Vignes, dated with ESR on teeth at 45 ka (Valladas et al., 1999), and El Esquilleu levels XI–XV (Rios-Garaizar, 2017). Across these sites, the chronological pattern consistently situates Quina occupations between MIS 5a and MIS 3.

If the maximum expression of the Quina system coincides with the cold cycles of MIS 4–3, the isolated development of certain technical features (analogous core-reduction systems and Quina retouching on scrapers) could be older, as documented from MIS 11–9 sites in the Levant (Barkai and Gopher, 2013), Balkans (Mihailović et al., 2022), and in Western Europe (Rose, 1992; Delpech et al., 1995). Finally, the first Quina technotypological system has

recently been discovered in a Middle Paleolithic site in Eastern Asia, with materials embedded in a deposit on a fluvial terrace, dated by OSL to a range between the end of MIS 4 and the early part of MIS 3 (approximately 60–50 ka) (Ruan et al., 2025), making the chronocultural analogy with European contexts noteworthy.

Furthermore, when examined alongside fauna-based climatic reconstructions for De Nadale, the U-S/ESR ages suggest occupation during a relatively cold phase (López-García et al., 2018). This is consistent with the presence of cold-adapted fauna at the site and supports interpretations that Neanderthal groups were resilient in response to climatic fluctuations.

Overall, the new dating results from De Nadale Cave enhance our understanding of Neanderthal occupation patterns in the Berici Mounts and contribute to broader debates on regional variability and cultural adaptation during the Middle Paleolithic. The alignment of our dating results with previous biochronological data, charcoal fragment analyses, and U-series dating lends further credibility to the robustness of the combined chronological framework (Jéquier et al., 2015; López-García et al., 2018; Livraghi et al., 2021, 2022; Vidal-Matutano et al., 2022). In particular, the agreement of multiple dating methods reinforces the reliability of the U-S/ESR technique in contexts where direct dating of archaeological material is often challenging (Joannes-Boyau, 2014; Duval and Grün, 2016). The age estimates support the idea that De Nadale was occupied during a transitional climate period, potentially reflecting adaptive responses by Neanderthal groups to environmental shifts. The confirmation of an MIS 5a/MIS 4 transition age for De Nadale adds weight to the emerging view that the Quina Mousterian was a widespread and temporally extended technocomplex, potentially reflecting demographic stability or repeated seasonal use of key locations across the landscape.

6. Conclusion

The chronological results from this study establish De Nadale Cave as a significant Middle Paleolithic Neanderthal occupation in the Berici Mounts region of Italy. The application of the U-S/ESR dating method, supported by other geochronological techniques, provides consistent and reliable age estimates, indicating that the site was occupied during the transitional period between late MIS 5 and the beginning of MIS 4. Although these ages are consistent with previous chronological constraints, some uncertainty remains, particularly related to the reconstruction of the environmental dose rate. These results not only demonstrate the applicability of U-S/ESR dating but also demonstrate its value in establishing direct chronologies for critical fossil- and artifact-bearing layers, particularly in complex archaeological contexts like the De Nadale Cave.

By refining the chronological framework of the site, this study provides important insights into Neanderthal occupation patterns and ecological strategies during a climatically unstable period. Together, the findings enhance our understanding of Neanderthal settlement dynamics in northern Italy during the MIS 5a–MIS 4 period and contribute to broader discussions on regional behavioral variability and adaptation to environmental change during the Middle Paleolithic.

Declaration of competing interest

The authors declare no conflicts of interest.

Acknowledgments

Research at De Nadale Cave is coordinated by the University of Ferrara (M.P.) within the framework of a project supported by the Ministry of Culture—Veneto Archaeological Superintendence and the Zovencedo Municipality—and financed by the University of Ferrara, the H. Obermaier Society, local private companies (R.A.A.S.M.), and local promoters. This research was also supported by the Australian Research Council Discovery Project grants (ARC DP140100919 and ARC DP220100195 to R.J.B. and ARC DP170100056 to R.J.B.), an Australian Research Council Linkage Infrastructure, Equipment and Facilities (LIEF) grant (ARC LE200100022 to R.J.B.), and an ARC Future Fellowship grant (ARC FT200100816 to M.D.). We thank Chuanyi Wei and Xingshuo Xu for their assistance with dose–response curves. The authors would like to thank Mathieu Duval for his constructive advice on closed system electron spin resonance age calculation. We are grateful to Jack Alexandrovics for his help with software troubleshooting. Southern Cross University generously contributed to the installation of the electron spin resonance spectrometer.

Author contributions

Wenjing Yu: Writing – review & editing, Writing – original draft, Software, Methodology, Investigation, Formal analysis. **Lee J. Arnold:** Writing – review & editing, Software, Resources, Methodology. **Martina Demuro:** Investigation, Data curation. **Davide Delpiano:** Writing – review & editing, Data curation. **Alessandra Livraghi:** Writing – review & editing, Methodology, Data curation. **Renaud Joannes-Boyau:** Writing – review & editing, Software, Methodology, Funding acquisition. **Marco Peresani:** Writing – review & editing, Validation, Resources, Project administration, Funding acquisition, Data curation, Conceptualization.

Supplementary Online Material

Supplementary Online Material related to this article can be found at https://doi.org/10.1016/j.jhevol.2026.103842.

References

Adamiec, G., Aitken, M.J., 1998. Dose-rate conversion factors: Update. Ancient TL 16 (2), 37–50.
Allkofer, O.C., 1975. Introduction to cosmic radiation. NASA STI/Recon Technical Report A 75, 46929.
Arnaud, J., Benazzi, S., Romandini, M., Livraghi, A., Panetta, D., Salvadori, P.A., Volpe, L., Peresani, M., 2017. A Neanderthal deciduous human molar with incipient carious infection from the Middle Palaeolithic De Nadale cave, Italy. Am. J. Phys. Anthropol. 162 (2), 370–376.
Arnold, L.J., Duval, M., Falguères, C., Bahain, J.-J., Demuro, M., 2012. Portable gamma spectrometry with cerium-doped lanthanum bromide scintillators: Suitability assessments for luminescence and electron spin resonance dating applications. Radiat. Meas. 47 (1), 6–18.
Bahain, J.-J., Duval, M., Voinchet, P., Tissoux, H., Falguères, C., Grün, R., Moreno, D., Shao, Q., Tombret, O., Jamet, G., Faivre, J.-P., Cliquet, D., 2020. ESR and ESR/U-series chronology of the Middle Pleistocene site of Tourville-la-Rivière (Normandy, France) - A multi-laboratory approach. Quatern. Int. 556, 66–78.
Bahain, J.-J., Voinchet, P., Vietti, A., Shao, Q., Tombret, O., Pereira, A., Nomade, S., Falguères, C., 2021. ESR/U-series and ESR dating of several Middle Pleistocene Italian sites: Comparison with 40Ar/39Ar chronology. Quatern. Geochronol. 63, 101151.
Barkai, R., Gopher, A., 2013. Cultural and biological transformations in the Middle Pleistocene Levant: A view from Qesem Cave, Israel. In: Dynamics of Learning in Neanderthals and Modern Humans, vol. 1. Cultural Perspectives, pp. 115–137.
Bassi, D., 2000. Shallow water benthic communities at the Middle-Upper Eocene boundary. Southern and north-eastern Italy, Slovenia, Croatia, Hungary. In: Field trip guidebook of the 5th meeting IGCP 393. IUGS-UNESCO.
Ben Arous, E., Falguères, C., Tombret, O., El Hajraoui, M.A., Nespoulet, R., 2020. Combined US-ESR dating of fossil teeth from El Harhoura 2 cave (Morocco): New data about the end of the MSA in Temara region. Quatern. Int. 556, 88–95.
Bertola, S., Peresani, M., 2000. Variabilità tecnologica in due insiemi litici di superficie dei Colli Berici. Quaderni di Archeologia del Veneto 16, 92–96.
Bertola, S., Peresani, M., Peretto, C., Thun Hohenstein, U., 1999. Le site paléolithique moyen de la Grotta della Ghiacciaia (Préalpes de Vénétie, Italie du Nord). L'Anthropologie 103 (3), 377–390.

Bischoff, J.L., Rosenbauer, R.J., 1981. Uranium series dating of human skeletal remains from the Del Mar and Sunnyvale sites, California. Science 213 (4511), 1003–1005.
Blackwell, B.A.B., Porat, N., Schwarcz, H.P., Debenath, A., 1992. ESR dating of tooth enamel: Comparison with 230Th234U speleothem dates at La Chaise-de-Vouthon (Charente), France. Quatern. Sci. Rev. 11 (1–2), 231–244.
Bordes, F., 1984. Le Paléolithique en Europe. Lecons sur le Paléolithique, II. Cah. Du. Quatern. 7.
Bordes, F., Bourgon, M., 1951. Le complexe Moustérien: Moustériens, levalloisien et tayacien. L'Anthropologie 55, 1–23.
Bourguignon, L., 1996. La conception de débitage Quina. Quatern. Nova VI, 149–196.
Bourguignon, L., 1997. Le Moustérien de Type Quina: Nouvelles Définitions d'une Entité Technique. Université de Paris X-Nanterre.
Brennan, B.J., Rink, W.J., McGuirl, E.L., Schwarcz, H.P., Prestwich, W.V., 1997. Beta doses in tooth enamel by 'one-group' theory and the ROSY ESR dating software. Radiat. Meas. 27 (2), 307–314.
Castel, J.-C., Discamps, E., Soulier, M.-C., Sandgathe, D., Dibble, H.L., McPherron, S.J.P., Goldberg, P., Turq, A., 2024. Neandertal subsistence strategies during the Quina Mousterian at Roc de Marsal (France). Quatern. Int. 433, 140–156.
Delpech, F., Geneste, J.-M., Rigaud, J.P., Texier, J.-P., 1995. Les industries antérieures à la dernière glaciation en Aquitaine septentrionale: Chronologie, paléoenvironnements, technologie, typologie et économie de subsistance. Paléo, Revue d'Archéologie Préhistorique 1 (1), 133–163.
Delpiano, D., Zupancich, A., Bertola, S., Martellotta, E.F., Livraghi, A., Cristiani, E., Peresani, M., 2022. Flexibility within Quina lithic production systems and tool-use in Northern Italy: Implications on Neanderthal behavior and ecology during early MIS 4. Archaeol. Anthropol. Sci. 14 (12), 219.
Demuro, M., Arnold, L.J., González-Urquijo, J., Lazuen, T., Frochoso, M., 2023. Chronological constraint of Neanderthal cultural and environmental changes in southwestern Europe: MIS 5–MIS 3 dating of the Axlor site (Biscay, Spain). J. Quatern. Sci. 38 (6), 891–920.
Dirks, P.H., Roberts, E.M., Hilbert-Wolf, H., Kramers, J.D., Hawks, J., Dosseto, A., Duval, M., Elliott, M., Evans, M., Grün, R., Hellstrom, J., Herries, A.I., Joannes-Boyau, R., Makhubela, T.V., Placzek, C.J., Robbins, J., Spandler, C., Wiersma, J., Woodhead, J., Berger, L.R., 2017. The age of Homo naledi and associated sediments in the Rising Star Cave, South Africa. eLife 6, e24231.
Duval, M., 2015. Electron spin resonance (ESR) dating of fossil tooth enamel. In: Jack Rink, W., Thompson, J.W. (Eds.), Encyclopedia of Scientific Dating Methods. Springer Netherlands, Dordrecht, pp. 239–246.
Duval, M., Arnold, L.J., 2013. Field gamma dose-rate assessment in natural sedimentary contexts using LaBr3(Ce) and NaI(Tl) probes: A comparison between the "threshold" and "windows" techniques. Appl. Radiat. Isot. 74, 36–45.
Duval, M., Arnold, L.J., Rixhon, G., 2020. Electron spin resonance (ESR) dating in Quaternary studies: Evolution, recent advances and applications. Quatern. Int. 556, 1–10.
Duval, M., Grün, R., 2016. Are published ESR dose assessments on fossil tooth enamel reliable? Quatern. Geochronol. 31, 19–27.
Duval, M., Grün, R., Falgueres, C., Bahain, J.-J., Dolo, J.-M., 2009. ESR dating of Lower Pleistocene fossil teeth: Limits of the single saturating exponential (SSE) function for the equivalent dose determination. Radiat. Meas. 44 (5–6), 477–482.
Duval, M., Guilarte Moreno, V., Grün, R., 2013. ESR dosimetry of fossil enamel: Some comments about measurement precision, long-term signal fading and dose–response curve fitting. Radiat. Protect. Dosim. 157 (4), 463–476.
Duval, M., Martin, L., 2019. ESR dating of fossil teeth: In which extent the thickness of adjacent tissues should be taken into account in the external beta dose rate evaluation? Geochronometria 46 (1), 102–110.
Falguères, C., Gruppioni, G., Bahain, J.J., Dolo, J.M., Peresani, M., 2025. Dating the Middle Palaeolithic of Fumane Cave by the combined ESR/U-series method. J. Quatern. Sci. 40, 862–875.
Fellows Yates, J.A., Velsko, I.M., Aron, F., Posth, C., Hofman, C.A., Austin, R.M., Parker, C.E., Mann, A.E., Nägele, K., Arthur, K.W., Arthur, J.W., Bauer, C.C., Crevecoeur, I., Cupillard, C., Curtis, M.C., Dalén, L., Díaz-Zorita Bonilla, M., Díez Fernández-Lomana, J.C., Drucker, D.G., Escribano Escrivá, E., Francken, M., Gibbon, V.E., González Morales, M.R., Grande Mateu, A., Harvati, K., Henry, A.G., Humphrey, L., Menéndez, M., Mihailović, D., Peresani, M., Rodríguez Moroder, S., Roksandic, M., Rougier, H., Sázelová, S., Stock, J.T., Straus, L.G., Svoboda, J., Teßmann, B., Walker, M.J., Power, R.C., Lewis, C.M., Sankaranarayanan, K., Guschanski, K., Wrangham, R.W., Dewhirst, F.E., Salazar-García, D.C., Krause, J., Herbig, A., Warinner, C., 2021. The evolution and changing ecology of the African hominid oral microbiome. Proc. Natl. Acad. Sci. 118 (20), e2021655118.
Frouin, M., Lahaye, C., Mercier, N., Guibert, P., Couchoud, I., Texier, J.P., Royer, A., Costamagno, S., Beauval, C., Bourguignon, L., Meignen, L., Bordes, J.G., Seguin, G., Bocherens, H., Lacrampe-Cuyaubère, F., Muth, X., Geigl, E.M., Grün, R., Garralda, M.D., Vandermeersch, B., Mann, A.E., Maureille, B., 2017a. Chronologie du site moustérien de type Quina des Pradelles (Marillac-le-Franc, Charente, France). Paléo 28, 117–136.
Frouin, M., Lahaye, C., Valladas, H., Higham, T., Debénath, A., Delagnes, A., Mercier, N., 2017b. Dating the Middle Paleolithic deposits of La Quina Amont (Charente, France) using luminescence methods. J. Hum. Evol. 109, 30–45.
Garralda, M.D., Le Cabec, A., Maíllo-Fernández, J.-M., Maureille, B., Gunz, P., Neira, A., Hublin, J.-J., Bernaldo de Quirós, F., 2023. Mousterian human fossils from El Castillo cave (Puente Viesgo, Cantabria, Spain). J. Anthropol. Sci. 101.
Grün, R., 2009. The DATA program for the calculation of ESR age estimates on tooth enamel. Quatern. Geochronol. 4 (3), 231–232.
Grün, R., Katzenberger-Apel, O., 1994. An alpha irradiator for ESR dating. Ancient TL 12 (2), 35–38.
Grün, R., Schwarcz, H.P., Chadam, J., 1988. ESR dating of tooth enamel: Coupled correction for U-uptake and U-series disequilibrium. Int. J. Radiat. Appl. Instrum. Nucl. Tracks Radiat. Meas. 14 (1–2), 237–241.
Guérin, G., Christophe, C., Philippe, A., Murray, A.S., Thomsen, K.J., Tribolo, C., Urbanova, P., Jain, M., Guibert, P., Mercier, N., Kreutzer, S., Lahaye, C., 2017. Absorbed dose, equivalent dose, measured dose rates, and implications for OSL age estimates: Introducing the Average Dose Model. Quatern. Geochronol. 41, 163–173.
Guérin, G., Discamps, E., Lahaye, C., Mercier, N., Guibert, P., Turq, A., Dibble, H.L., McPherron, S.P., Sandgathe, D., Goldberg, P., 2012. Multi-method (TL and OSL), multi-material (quartz and flint) dating of the Mousterian site of Roc de Marsal (Dordogne, France): Correlating Neanderthal occupations with the climatic variability of MIS 5–3. J. Archaeol. Sci. 39 (10), 3071–3084.
Hakim, B., Wibowo, U.P., van den Bergh, et al., 2025. Hominins on Sulawesi during the Early Pleistocene. Nature 646, 378–383.
Han, F., Bahain, J.-J., Deng, C., Boëda, É., Hou, Y., Wei, G., Huang, W., Garcia, T., Shao, Q., He, C., Falguères, C., Voinchet, P., Yin, G., 2017. The earliest evidence of hominid settlement in China: Combined electron spin resonance and uranium series (ESR/U-series) dating of mammalian fossil teeth from Longgupo cave. Quatern. Int. 434, 75–83.
Han, F., Shao, Q., Bahain, J.-J., Sun, X., Yin, G., 2019. Coupled ESR and U-series dating of Middle Pleistocene hominin site Bailongdong cave, China. Quatern. Geochronol. 49, 291–296.
Herries, A.I.R., Murszewski, A., Pickering, R., Mallett, T., Joannes-Boyau, R., Armstrong, B., Adams, J.W., Baker, S., Blackwood, A.F., Penzo-Kajewski, P., Kappen, P., Leece, A., Martin, J., Rovinsky, D., Boschian, G., 2018. Geo-archaeological and 3D visualisation approaches for contextualising in-situ fossil bearing palaeokarst in South Africa: A case study from the ~2.61 Ma Drimolen Makondo. Quatern. Int. 483, 90–110.
Ikeya, M., 1982. A model of linear uranium accumulation for ESR age of Heidelberg (Mauer) and Tautavel bones. Jpn. J. Appl. Phys. 21 (11A), L690.
Jacobs, Z., Jankowski, N.R., Dibble, H.L., Goldberg, P., McPherron, S.J.P., Sandgathe, D., Soressi, M., 2016. The age of three Middle Palaeolithic sites: Single-grain optically stimulated luminescence chronologies for Pech de l'Azé I, II and IV in France. J. Hum. Evol. 95, 80–103.
Jéquier, C., Peresani, M., Romandini, M., Delpiano, D., Joannes-Boyau, R., Lembo, G., Livraghi, A., López-García, J.M., Obradović, M., Nicosia, C., 2015. The De Nadale Cave, a single layered Quina Mousterian site in the North of Italy. Quartär 62, 7–21.
Joannes-Boyau, R., 2014. Electron spin resonance (ESR) dating in archaeology. In: Smith, C. (Ed.), Encyclopedia of Global Archaeology. Springer, New York, pp. 2352–2358.
Joannes-Boyau, R., Duval, M., Bodin, T., 2018. MCDoseE 2.0 A new Markov Chain Monte Carlo program for ESR dose response curve fitting and dose evaluation. Quatern. Geochronol. 44, 13–22.
Joannes-Boyau, R., Grün, R., Bodin, T., 2010. Decomposition of the laboratory gamma irradiation component of angular ESR spectra of fossil tooth enamel fragments. Appl. Radiat. Isot. 68 (9), 1798–1808.
Joannes-Boyau, R., de Souza, J.S., Arora, M., Austin, C., Westaway, K., Moffat, I., Wang, W., Liao, W., Zhang, Y., Adams, J.W., Fiorenza, L., Dérognat, F., Moncel, M.-H., Schwartz, G.T., Bailey, M., dos Santos, F.F., Guardia, G.D.A., Mercuri, R.L.V., Galante, P.A.F., Martins, A.M.A., Tsu, B.L., Barnes, C.A., Yates, J., Petroski, L.P., Sanchez-Sanchez, S.M., Oviedo, J., Herai, R.H., Lemos, B., Tonge, M., Muotri, A.R., 2025. Impact of intermittent lead exposure on hominid brain evolution. Sci. Adv. 11 (42), eadr1524.
Laville, H., 1973. The relative position of Mousterian Industries in the climatic chronology of the early Wurm in the Perigord. World Archaeol. 4 (3), 323–329.
Leslie, C., 2009. Analysing Environmental Radioactivity in Soils and Sediments Using High-purity Germanium Gamma Detectors at CSIRO Land and Water: Procedures and Protocols. CSIRO.
Liberda, J.J., Thompson, J.W., Rink, W.J., Bernaldo de Quirós, F., Jayaraman, R., Selvaretinam, K., Chancellor-Maddison, K., Volterra, V., 2010. ESR dating of tooth enamel in Mousterian layer 20, El Castillo, Spain. Geoarchaeology 25 (4), 467–474.
Lisiecki, L.E., Raymo, M.E., 2005. A Pliocene-Pleistocene stack of 57 globally distributed benthic δ18O records. Paleoceanography 20 (1).
Livraghi, A., Fanfarillo, G., Colle, M.D., Romandini, M., Peresani, M., 2021. Neanderthal ecology and the exploitation of cervids and bovids at the onset of MIS4: A study on De Nadale cave, Italy. Quatern. Int. 586, 24–41.
Livraghi, A., Rivals, F., Rendu, W., Peresani, M., 2022. Neanderthals' hunting seasonality inferred from combined cementochronology, mesowear, and microwear analysis: Case studies from the Alpine foreland in Italy. Archaeol. Anthropol. Sci. 14 (3), 51.
López-García, J.M., Livraghi, A., Romandini, M., Peresani, M., 2018. The De Nadale Cave (Zovencedo, Berici Hills, northeastern Italy): A small-mammal fauna from near the onset of Marine Isotope Stage 4 and its palaeoclimatic implications. Palaeogeogr. Palaeoclimatol. Palaeoecol. 506, 196–201.
Margaritora, D., Dozio, A., Chelidonio, G., Turrini, M.C., Peresani, M., 2020. The Lower and Middle Palaeolithic settlements in the Baldo-Lessini mountains. Results from a GIS investigation. Alp. Mediterr. Quatern. 33 (1), 115–132.

Martellotta, E.F., Livraghi, A., Delpiano, D., Peresani, M., 2021. Bone retouchers from the Mousterian Quina site of De Nadale Cave (Berici Hills, north-eastern Italy). J. Archaeol. Sci. Rep. 36, 102864.
Maureille, B., Mann, A.E., Beauval, C., Bordes, Jean-Guillaume, Bourguignon, L., Sandrine, C., Couchoud, I., Garralda, M.D., Geigl, E.-M., Fouquignon, J., Lacrampe-Cuyaubère, F., Grün, R., Guibert, P., Laroulandie, V., Marquet, J.-C., Meignen, L., Mussini, C., Rendu, W., Royer, A., Seguin, G., Texier, J.-P., 2010. Les Pradelles à Marillac-le-Franc (Charente). Fouilles 2001-2007: Nouveaux résultats et synthèse. In: Préhistoire entre Vienne et Charente. Hommes et sociétés du Paléolithique. Association des Publications Chauvinoises, pp. 145–162.
Michel, V., Shen, G., Valensi, P., de Lumley, H., 2009. ESR dating of dental enamel from Middle Palaeolithic levels at Lazaret Cave, France. Quatern. Geochronol. 4 (3), 233–240.
Mietto, P., 1988. Aspetti geologici dei Monti Berici. In: VV, A.A. (Ed.), I Colli Berici, Natura e Civiltà. Signum, Padua, Italy, pp. 12–23.
Mietto, P., Sauro, U., 2000. Le Grotte Del Veneto: Paesaggi Carsici e Grotte Del Veneto, seconda edizione. Regione del Veneto-La Grafica Editrice, Verona.
Mihailović, D., Milošević, S., Blackwell, B.A.B., Mercier, N., Mentzer, S.M., Miller, C.E., Morley, M.W., Bogićević, K., Đurić, D., Marković, J., Mihailović, B., Dragosavac, S., Plavšić, S., Skinner, A.R., Chaity, I.I.C., Huang, Y.E.W., Chu, S., Nenadić, D., Radović, P., Lindal, J., Roksandic, M., 2022. Neanderthal settlement of the Central Balkans during MIS 5: Evidence from Pešturina Cave, Serbia. Quatern. Int. 610, 1–19.
Mihailović, D., Whallon, R., 2017. Crvena Stijena revisited: The late Mousterian assemblages. Quatern. Int. 450, 36–49.
Nava, A., Lugli, F., Romandini, M., Badino, F., Evans, D., Helbling, A.H., Oxilia, G., Arrighi, S., Bortolini, E., Delpiano, D., Duches, R., Figus, C., Livraghi, A., Marcini, G., Silvestrini, S., Cipriani, A., Giovanardi, T., Pini, R., Tuniz, C., Bernardini, F., Dori, I., Coppa, A., Cristiani, E., Dean, C., Bondioli, L., Peresani, M., Müller, W., Benazzi, S., 2020. Early life of Neanderthals. Proc. Natl. Acad. Sci. U.S.A. 117 (46), 28719–28726.
Pereira, A., Nomade, S., Falguères, C., Bahain, J.-J., Tombret, O., Garcia, T., Voinchet, P., Bulgarelli, G.-M., Anzidei, A.-P., 2017. 40Ar/39Ar and ESR/U-series data for the La Polledrara di Cecanibbio archaeological site (Lazio, Italy). J. Archaeol. Sci. Rep. 15, 20–29.
Peresani, M., 2001. An overview of the Middle Palaeolithic settlement system in North-Eastern Italy. In: Conard, N.J. (Ed.), Settlement Dynamics of the Middle Palaeolithic and Middle Stone Age. Kerns Verlag, Tübingen, pp. 485–506.
Peresani, M., 2012. Fifty thousand years of flint knapping and tool shaping across the Mousterian and Uluzzian sequence of Fumane cave. Quatern. Int. 247, 125–150.
Peresani, M., 2015. I Neandertaliani e il Musteriano nei Colli Berici. Insediamenti e sfruttamento delle materie prime litiche. Archeol. Veneta XXXVIII, 10–27.
Peresani, M., 2022. Inspecting human evolution from a cave. Late Neanderthals and early sapiens at Grotta di Fumane: Present state and outlook. J. Anthropol. Sci. 100, 71–107.
Peresani, M., 2023. Adaptations and cultures of Pleistocene humans in Italy. Alp. Mediterr. Quatern. 36 (2), 185–204.
Peresani, M., Bourguignon, L., Delpiano, D., Lemorini, C., 2023. Quina on the edge. Insights from a Middle Palaeolithic lithic assemblage of Grotta di Fumane, Italy. J. Archaeol. Sci. Rep. 49, 103998.
Prescott, J.R., Hutton, J.T., 1994. Cosmic ray contributions to dose rates for luminescence and ESR dating: Large depths and long-term time variations. Radiat. Meas. 23 (2–3), 497–500.
Richard, M., Falguères, C., Pons-Branchu, E., Richter, D., Beutelspacher, T., Conard, N.J., Kind, C.-J., 2020. The Middle to Upper Palaeolithic transition in Hohlenstein-Stadel cave (Swabian Jura, Germany): A comparison between ESR, U-series and radiocarbon dating. Quatern. Int. 556, 49–57.
Richard, M., Moreno, D., Bahain, J.-J., Duval, M., Falguères, C., 2017. Electron spin resonance dating of fossil teeth: Some basic guidelines to ensure optimal sampling conditions. Quaternaire 28 (2), 155–159.
Richter, D., Grün, R., Joannes-Boyau, R., Steele, T.E., Amani, F., Rué, M., Fernandes, P., Raynal, J.-P., Geraads, D., Ben-Ncer, A., Hublin, J.-J., McPherron, S.P., 2017. The age of the hominin fossils from Jebel Irhoud, Morocco, and the origins of the Middle Stone Age. Nature 546 (7657), 293–296.
Richter, D., Hublin, J.-J., Jaubert, J., McPherron, S.P., Soressi, M., Texier, J.-P., 2013. Thermoluminescence dates for the Middle Palaeolithic site of Chez-Pinaud Jonzac (France). J. Archaeol. Sci. 40 (2), 1176–1185.
Rios-Garaizar, J., 2017. A new chronological and technological synthesis for Late Middle Paleolithic of the Eastern Cantabrian Region. Quatern. Int. 433, 50–63.
Rizal, Y., Westaway, K.E., Zaim, Y., van den Bergh, G.D., Bettis, E.A., Morwood, M.J., Huffman, O.F., Grün, R., Joannes-Boyau, R., Bailey, R.M., 2020. Last appearance of *Homo erectus* at Ngandong, Java, 117,000–108,000 years ago. Nature 577 (7790), 381–385.
Rolland, N., 1981. The interpretation of Middle Palaeolithic variability. Man 15–42.
Rose, J., 1992. High Lodge-regional context and geological background. In: Ashton, N., Cook, J., Lewis, S., Rose, J. (Eds.), High Lodge: Excavations by G. de G. Sieveking, 1962–1968 and J. Cook, 1988, pp. 13–24. London.
Ruan, Q.-J., Li, H., Xiao, P.-Y., Li, B., Monod, H., Sumner, A., Zhao, K.-L., Liu, J.-H., Jia, Z.-X., Wang, C.-X., 2025. Quina lithic technology indicates diverse Late Pleistocene human dynamics in East Asia. Proc. Natl. Acad. Sci. 122 (14), e2418029122.
Sauro, U., 2005. The Monti Berici: Guide of the fieldtrip. Suppl. Geogr. Fis. Din. Quaternaria 7.
Sauro, U., 2016. The Monti Berici: A peculiar type of karst in the Southern Alps. KIP Articles 31 (3).
Shao, Q., 2011. Combined ESR/U-series dating of fossil teeth from middle Pleistocene sites in northern Europe and Mediterranean area: Contributing to the chronology of the Acheulian settlement of Europe. Ph.D Thesis. Muséum national d'Histoire naturelle, Paris.
Shao, Q., Bahain, J.-J., Dolo, J.-M., Falguères, C., 2014. Monte Carlo approach to calculate US-ESR age and age uncertainty for tooth enamel. Quatern. Geochronol. 22, 99–106.
Slimak, L., Vimala, T., Seguin-Orlando, A., Metz, L., Zanolli, C., Joannes-Boyau, R., Frouin, M., Arnold, L.J., Demuro, M., Devièse, T., Comeskey, D., Buckley, M., Camus, H., Muth, X., Lewis, J.E., Bocherens, H., Yvorra, P., Tenailleau, C., Duployer, B., Coqueugniot, H., Dutour, O., Higham, T., Sikora, M., 2024. Long genetic and social isolation in Neanderthals before their extinction. Cell Genom. 4 (9), 100593.
Slimak, L., Zanolli, C., Higham, T., Frouin, M., Schwenninger, J.-L., Arnold, L.J., Demuro, M., Douka, K., Mercier, N., Guérin, G., 2022. Modern human incursion into Neanderthal territories 54,000 years ago at Mandrin, France. Sci. Adv. 8 (6), eabj9496.
Smith, M.A., Prescott, J.R., Head, M.J., 1997. Comparison of 14C and luminescence chronologies at Puritjarra rock shelter, central Australia. Quatern. Sci. Rev. 16 (3–5), 299–320.
Terlato, G., Livraghi, A., Romandini, M., Peresani, M., 2019. Large bovids on the Neanderthal menu: Exploitation of *Bison priscus* and *Bos primigenius* in northeastern Italy. J. Archaeol. Sci. Rep. 25, 129–143.
Terlato, G., Lubrano, V., Romandini, M., Marín-Arroyo, A.B., Benazzi, S., Peresani, M., 2021. Late Neanderthal subsistence at san bernardino cave (berici hills-northeasternitaly) inferred from zooarchaeological data: Neanderthal subsistence in northeastern Italy. Alp. Mediterr. Quatern. 34 (2), 213–235.
Turq, A., 1989. Approche technologique et économique du faciès Moustérien de type Quina: Étude préliminaire. Bull. Soc. Prehist. Fr. 244–256.
Turq, A., 2000. Le moustérien de type Quina. Paléo, Revue d'Archéologie Préhistorique 2 (1), 310–343.
Tusberti, F., Chimento, F., Brandano, M., Breda, A., Massironi, M., Luisa Perissinotto, M., Tomassetti, L., Preto, N., 2024. Geometry and stratigraphic relationships of lower Oligocene coral reefs in Lumignano (Berici Hills, northern Italy). Ital. J. Geosci. 143 (1), 25–36.
Valladas, H., Mercier, N., Froget, L., Hovers, E., Joron, J.-L., Kimbel, W.H., Rak, Y., 1999. TL dates for the Neanderthal site of the Amud Cave, Israel. J. Archaeol. Sci. 26 (3), 259–268.
Valladas, H., Mercier, N., Joron, J.L., McPherron, S.P., Dibble, H.L., Lenoir, M., 2003. TL dates for the middle paleolithic site of Combe-Capelle Bas, France. J. Archaeol. Sci. 30 (11), 1443–1450.
Verna, C., Dujardin, V., Trinkaus, E., 2012. The Early Aurignacian human remains from La Quina-Aval (France). J. Hum. Evol. 62 (5), 605–617.
Vidal-Matutano, P., Livraghi, A., Peresani, M., 2022. New charcoal evidence at the onset of MIS 4: First insights into fuel management and the local landscape at De Nadale cave (northeastern Italy). Rev. Palaeobot. Palynol. 298, 104594.
Withnell, C.B., Joannes-Boyau, R., Bell, C.J., 2020. A reassessment of the age of the fauna from Cumberland Bone Cave, Maryland, (middle Pleistocene) using coupled U-series and electron spin resonance dating (ESR). Quatern. Res. 97, 187–198.
Yu, W., Herries, A.I.R., Edwards, T., Armstrong, B., Joannes-Boyau, R., 2024. Combined uranium-series and electron spin resonance dating from the Pliocene fossil sites of Aves and Milo's palaeocaves, Bolt's Farm, Cradle of Humankind, South Africa. PeerJ 12, e17478.
Yu, W., Herries, A.I.R., Joannes-Boyau, R., 2025. The challenges of direct dating of fossil teeth from the *Australopithecus africanus*, Taung Child type site, South Africa. Quatern. Geochronol. 90, 101696.